Artemisinin and its derivatives target mitochondrial c-type cytochromes in yeast and human cells

Anais Laleve, Cristina Panozzo, Inge Kühl, Alexa Bourand-Plantefol, Jelena Ostojic, Abdoulaye Sissoko, Déborah Tribouillard-Tanvier, David Cornu, Angélique Burg, Brigitte Meunier, et al.

Artemisinin and its derivatives target mitochondrial *c*-type cytochromes in yeast and human cells.

Anais Laleve[a,1,*], Cristina Panozzo[a], Inge Kühl[a], Alexa Bourand-Plantefol[a], Jelena Ostojic[a,2], Abdoulaye Sissoko[b], Déborah Tribouillard-Tanvier[c,3], David Cornu[a], Angélique Burg[a], Brigitte Meunier[a], Marc Blondel[c], Jerome Clain[b], Nathalie Bonnefoy[a], Romain Duval[b], Geneviève Dujardin[a,*].

[a]Université Paris-Saclay, CEA, CNRS, Institute for Integrative Biology of the Cell (I2BC), 91198, Gif-sur-Yvette, France.

[b]Université de Paris, MERIT, IRD, 4 Avenue de l'Observatoire, 75006 Paris, France.

[c]Inserm UMR1078, Université de Bretagne Occidentale, Faculté de Médecine et des Sciences de la Santé; Etablissement Français du Sang (EFS) Bretagne; CHRU Brest, Hôpital Morvan, Laboratoire de Génétique Moléculaire, 22 avenue Camille Desmoulins, 29200 Brest, France.

[*]Co-corresponding author. Email addresses: anais.laleve@gmail.com (A. Laleve) or genevieve.dujardin@i2bc.paris-saclay.fr (G. Dujardin)

[1]Present address: Université Paris-Saclay, AgroParis Tech, INRA, BIOGER UMR 1290, Thiverval-Grignon, France.

[2]Present address: Peptide Biology Laboratories, The Salk Institute for Biological Studies, La Jolla, CA 92037, USA.

[3]Present address: Institut de Biochimie et Génétique Cellulaires, CNRS UMR5095, Université de Bordeaux, 1 rue Camille Saint-Saëns, 33077 Bordeaux cedex, France.

Highlights

Artemisinin derivatives can compensate for a yeast *bcs1* mutation.

Artemisinin derivatives impair cytochrome *c1* maturation in yeast and human cells.

A fluorescent di-hydroartemisinin rapidly labels yeast and human mitochondria.

A fluorescent di-hydroartemisinin targets mitochondrial *c*-type cytochromes.

Di-hydroartemisinin binds covalently to heme of reduced cytochrome *c*.

Graphical Abstract

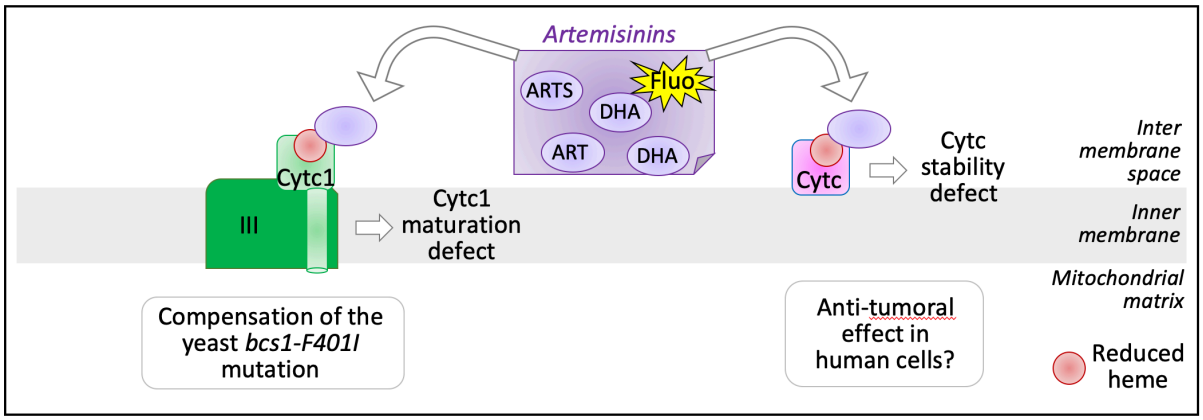

Abstract

Artemisinin and its derivatives kill malaria parasites and inhibit the proliferation of cancer cells. In both processes, heme was shown to play a key role in artemisinin bioactivation. We found that artemisinin and clinical artemisinin derivatives are able to compensate for a mutation in the yeast Bcs1 protein, a key chaperon involved in biogenesis of the mitochondrial respiratory complex III. The equivalent Bcs1 variant causes an encephalopathy in human by affecting complex III assembly. We show that artemisinin derivatives decrease the content of mitochondrial cytochromes and disturb the maturation of the complex III cytochrome *c1*. This last effect is likely responsible for the compensation by decreasing the detrimental over-accumulation of the inactive pre-complex III observed in the *bcs1* mutant. We further show that a fluorescent dihydroartemisinin probe rapidly accumulates in the mitochondrial network and targets cytochromes *c* and *c1* in yeast, human cells and isolated mitochondria. *In vitro* this probe interacts with purified cytochrome *c* only under reducing conditions and we detect cytochrome *c*-dihydroartemisinin covalent adducts by mass spectrometry analyses. We propose that reduced mitochondrial *c*-type cytochromes act as both early targets and mediators of artemisinin bioactivation in yeast and human cells.

Keywords: Mitochondria, *c*-Type cytochromes, Artemisinins, Fluorescent probe, Bcs1

1. Introduction

Artemisinin (ART) is a potent anti-malarial drug isolated from the plant *Artemisia annua*, and a series of clinical ART derivatives have been semi-synthesized including dihydroartemisinin (DHA), artemether (ARTMT), arteether (ARTET) and artesunate (ARTS) (for reviews, [1, 2]). Their anti-malarial action is a two-step process within the eukaryotic parasitic cell. First, artemisinins are activated by reductive cleavage of the endoperoxide pharmacophore bond to generate artemisinin radicals, and in *Plasmodium falciparum* heme would be predominantly responsible for this bioactivation. In a second step, the ART radicals irreversibly alkylate numerous parasite proteins, thereby compromising the parasite viability [3-8]. Studies performed in the malaria parasite and in the yeast *Saccharomyces cerevisiae* have shown that mitochondria may also play an important role in the mode of action of ART derivatives. The respiratory complexes might deliver reducing equivalents for the activation of the endoperoxide bond of the drug, causing ROS production and depolarization of mitochondrial membranes ([9-11] and for review [12]). In addition to their action against malaria, ART and derivatives are active against cancer cells in which they also target many proteins involved in critical biological pathways. In human cancer cells, it has been proposed that heme-dependent endoperoxide bioactivation would also take place in the mitochondria, generating oxidative stress and ROS production ([13-18] and for reviews [19-21]). Thus, both heme and mitochondria appear to play an important role in the action of ART and its derivatives in diverse eukaryotic cells.

Heme is an essential cofactor of mitochondrial cytochromes that are key components of the mitochondrial oxidative phosphorylation (OXPHOS) chain, which provides most of the ATP in non-plant cells. Cytochromes play the role of either mobile transporter like cytochrome *c* or catalytic membrane subunits of the two respiratory complexes III or IV (for review [22]). In these cytochromes, heme can be covalently attached like in *c*-type cytochromes, *c* and *c1*, or interact by electrostatic or hydrophobic interactions like in cytochromes *b* and *a*+*a3*

(for review [23]). Complex III contains the two types of cytochromes, *c1* and *b,* and is assembled through a dynamic modular pathway (for review [24]). The mitochondrial chaperon Bcs1 is required at a late step of assembly of complex III and its absence leads to the accumulation of an inactive pre-complex III [25-29]. Mutations in the human gene *BCS1L* are the most frequent nuclear mutations that lead to complex III-related pathologies and they are associated with very disparate clinical phenotypes (*e.g.* [30-36]). By screening the Prestwick® and BIOMOL® chemical libraries, we have identified several molecules able to compensate for the respiratory deficiency of *bcs1* mutations in yeast. The first class of compensatory molecules contains two antibiotics that target the mitochondrial rRNA and lead to an imbalanced synthesis of respiratory subunits that would modify the equilibrium between illegitimate inactive and active supercomplexes III/IV [37].

In this paper, we show that ART, ARTS, DHA, as well as a synthetic derivative of DHA covalently attached to a fluorophore (Fluo-DHA) are able to compensate for a yeast *bcs1* defect and we identify *c*-type cytochromes as key elements that not only mediate the action of artemisinins in the *bcs1* mutant but can also explain the anti-tumoral effect of these drugs in human cells.

2. Materials and methods

2.1. Chemicals

Artemisinin (ART, ref. 361593), dihydroartemisinin (DHA, ref. D7439), artesunate (ARTS, ref. A3731), hydrogen peroxide (ref. 216763) and dithiothreitol (DTT, ref. D9779) were purchased from Sigma Aldrich. Fluo-DHA (Sissoko *et al.*, submitted to ACS Infectious Diseases) corresponds to an HPA-NBD (4-(1'-hydroxypropyl-3'-amino)-7-nitrobenzoxadiazole) spacer-fluorophore moiety attached onto the C-10 center of DHA. ART and derivatives, including Fluo-DHA were all solubilized in DMSO.

Equine heart cytochrome *c* (Sigma Aldrich C7752) was prepared in 100 mM phosphate buffer at pH 7.4. This cytochrome *c* is mainly oxidized. To obtain the fully reduced form, 62 mg of cytochrome *c* were mixed with 4.5 mg of ascorbate, purified on a Sephadex G25 gel filtration column and aliquots were stored at -80°C. The level of reduction of each cytochrome *c* aliquot was systematically controlled after defrosting, by comparing the absorbance at 550 nm, before and after addition of ascorbate.

2.2. Yeast media and strain construction

Yeast media were prepared as in [38]. The fermentable medium used for all liquid cultures contains 2% galactose and a limited amount of glucose (0.1%) to avoid glucose repression of genes encoding mitochondrial proteins. Halo tests were performed as in [39] using solid respiratory medium containing 2% glycerol and 2% agar. Each single mutant was constructed by deleting the open reading frame (ORF) of the gene of interest in the wild-type strain CW252 (*MATalpha ade2-1 ura3-1 his3-11,15 trp1-1 leu2-3,112 can1-100*) [40]. The *bcs1*-F401I mutant has been described previously [29]. The Δ*cyt1* mutant is deprived of cytochrome *c1* (Δ*c1)*. In *S. cerevisiae*, there are two two isoforms of cytochrome *c* (Cyc1 and Cyc7) and two heme lyases: the cytochrome *c1* heme lyase Cyt2 and the cytochrome *c* heme lyase Cyc3; therefore, we

generated the double mutants Δ*cyc1*Δ*cyc7* (named Δ*c*) and Δ*cyt2*Δ*cyc3* (named Δ*hl*). These were thus constructed by crossing the single mutants of opposite mating type and dissecting tetrads using a Singer MSM micromanipulator. Since the *bcs1*-F401I mutant spontaneously generated revertants that grew faster on respiratory medium, we systematically verified that the level of revertants was less than 1% in each liquid culture before validating any data.

2.3. Whole yeast cell respiratory analyses

O_2 consumption was measured polarographically at room temperature using an oxygraph (Oxytherm, Hansatech) equipped with a Clark electrode, prepared according to the manufacturer's recommendations. $3x10^9$ cells grown in galactose medium for 2 days were added to the chamber containing 1 mL of fresh galactose medium and O_2 consumption was recorded for about 5 min. The rate of respiration was estimated by calculating the ratio of O_2 consumption to the cell amount (nM O_2/min/10^7 cells).

2.4. Yeast cytochrome spectra

Cytochrome spectra were recorded with a Cary 400 (Varian, San Fernando, CA) spectrophotometer at low temperature, from dried whole yeast cells supplemented with the reducing agent sodium hydrosulfite just before freezing in liquid nitrogen. For each spectrum, 10^{10} cells (OD_{600}=6) grown in liquid galactose medium without or with 1, 3 or 10 µM ARTS were used. A wt absorption spectra shows four main peaks corresponding to the cytochromes *c*, cytochromes *c1* and *b* of complex III and cytochrome *a+a3* of complex IV at 546, 552, 558 and 602 nm respectively.

2.5. Human cell culture

Unless otherwise indicated, human embryonic kidney cell lines (HEK293T/17, ATCC® CRL-11268™) were cultured in Dulbecco's modified Eagle's medium containing 25 mM glucose (DMEM, GlutaMax, Thermo Fisher Scientific, 31966–047), supplemented with 10% fetal bovine serum (Thermo Fisher Scientific, 10270–106) and 1% Penicillin/Streptomycin (Thermo Fisher Scientific, 15070–063) at 37 °C under a 5% CO_2 humidified atmosphere for a week, in six well plates with increasing concentrations of ARTS. Cells were tested for the presence of mycoplasma using the MycoAlert™ PLUS Mycoplasma Detection kit (LONZA, LT07-701).

To determine the IC_{50} of ARTS (the concentration of ARTS that inhibited growth by 50%) and its toxic dose, HEK293T cells were grown for a week in DMEM medium containing increasing concentrations of ARTS (from 0 to 10 µM). Cells were harvested and counted with an automated cell counter (Bio-Rad, TC20™). Under our conditions, the IC_{50} was between 3 and 5 µM and ARTS compromised cell survival above 8 µM.

2.6. Mitochondria purifications and total protein extractions

Yeast cells were grown for 24 h in galactose medium with or without ARTS and mitochondria were purified by differential centrifugation after digestion of the cell walls with Zymoliase-100T according to [41] except that a protease inhibitor cocktail (Roche) was added all along the purification to avoid the degradation of pre-complexes III/IV.

Human mitochondria were isolated from cultured HEK293T cells harvested and collected by centrifugation (800 g, 7 min, 4 °C) before resuspension in buffer A (70 mM sucrose, 20 mM HEPES pH 7.6, 220 mM mannitol, 1 mM EDTA and 2 mg/ml BSA) supplemented with protease inhibitor (Roche). The samples were incubated on ice (20 min) and homogenized in a drill fitted pestle for 30 strokes. Homogenates were centrifuged (800 g, 7 min, 4 °C) and the supernatant was removed and subjected to centrifugation at

10,000 g for 10 min (4 °C). Crude mitochondrial pellets were resuspended in buffer B (70 mM sucrose, 20 mM HEPES pH 7.6, 220 mM mannitol, 1 mM EDTA) supplemented with protease inhibitor (Roche) [42]. Total human proteins were extracted from cell pellets after a wash in cold DPBS (Thermo Fisher Scientific, 14190-250), lysis in SDS loading dye (100 mM Tris pH 6.8, 4% SDS, 20% glycerol, 200 mM DTT), incubation at 95°C for 5 min and sonication with a VibraCell™ (75042, Bioblock Scientific) apparatus (6 cycles of 5 s ON, 5 s OFF, at 20-30% amplitude).

2.7. SDS-PAGE, BN-PAGE and Western blot analyses

50 µg of mitochondrial proteins or total proteins extracted from 10^5 HEK cells were separated by SDS-PAGE (using 4–12% precast gels from Invitrogen) and then transferred, either directly or after fluorescence imaging (see below), onto a nitrocellulose membrane (GE Healthcare, Lifescience, Amersham). For BN-PAGE, the same amounts of mitochondria were lysed in a buffer containing 2% digitonin and mitochondrial complexes were separated on 3-12 BN-PAGE according to [41].

Immunodetection was performed according to standard techniques using enhanced chemiluminescence detection (Chemidoc, Bio Rad). Antibodies against yeast proteins were: (1) the in-house polyclonal antibodies: anti-Cytc (1/30,000), anti-Cyt1 (1/30,000), anti-Cytb (1/5,000) and anti-Nam1 (1/5,000), (2) the polyclonal antibodies anti-Atp1 (1/10000) from J. Velours, (Bordeaux, France) and anti-Rip1 (1/3000) from N. Fisher (Liverpool, UK) and (3) the monoclonal antibodies anti-Cox1 and anti-Cox2 (Abcam, 1/5,000 or 1/2000, respectively). For the detection of human proteins, the monoclonal anti-cytochrome *c* (CYCS, 1/1,000) and the polyclonal anti-cytochrome *c1* (CYC1, 1/5,000) were from Abcam; the monoclonal anti-Tom40 (1/1,000) was from Santa Cruz Biotechnology and the monoclonal anti-Tubulin (1/10,000) was from Sigma Aldrich.

2.8. Fluorescence gel imaging and microscopy

Proteins were separated by SDS-PAGE and the gel was directly visualized with a Typhoon Trio fluorescence imager (excitation 488 nm emission 555 nm). The optimal amounts of Fluo-DHA for yeast or human cells or mitochondria as well as of purified cytochrome *c* were determined in function of the IC_{50} for *in vivo* experiments and in line with the sensitivity of the fluorescent imager (data not shown). The amount of fluorescence was quantified using the Fiji software.

Yeast cells grown overnight in galactose liquid medium were incubated with 100 nM MitoTracker® Red CMXRos (Molecular Probes) for 30 min, washed and diluted in phosphate buffered saline (PBS) before addition of 3 µM Fluo-DHA and incubation for up to 30 min. Time-lapse fluorescence imaging of live cells was performed using a Nipkow Spinning Disk confocal device (Yokogawa CSU-X1-A1) mounted on Nikon Eclipse Ti E inverted microscope equipped with a 100 X APO TIRF oil immersion objective (Numerical Aperture (NA): 1.49). Blue (488 nm Vortran laser, 150 mW) and yellow (561 nm Vortran laser, 100 mW) lasers were used for excitation of the Fluo-DHA and MitoTracker® respectively. A quad band dichroic mirror 405/488/561/647 nm (Chroma) was used and band pass filters 525/545 nm and 607/636 nm (Semrock) allowed the detection of the Fluo-DHA and MitoTracker® respectively. For detection, a LiveSR module (GATACA systems) was placed above the Prime 95B sCMOS camera (Photometrics) to reach a two-fold increase in maximal resolution, and the whole system was driven by MetaMorph software version 7.10 (Molecular Devices).

HEK293T cells were grown for two days on a glass coverslip in low glucose DMEM medium, washed in PBS and incubated for 5 h with 5 µM Fluo-DHA. The cells were washed and incubated with 100 nM MitoTracker® for 30 min in the dark at 37 °C. After washing,

HEK293T cells were fixed using 4% paraformaldehyde in PBS, incubated for 30 min, washed and then the coverslip was placed on the slide using Vectashield mounting medium (Vector Labs) that preserves fluorescence and prevents rapid photoblenching of fluorescent molecules. Images were acquired with a Leica SP8X inverted confocal laser scanning microscope, equipped with a 63x HC Plan Apochromat CS2 oil-immersion objective (NA: 1.4). Mitotracker® Red was excited at 578 nm and detected between 590/640 nm while Fluo-DHA was excited at 488 nm and detected between 500/550 nm. Samples were illuminated sequentially and the emission was collected on GaAsP Hybrid (Hamamatsu) detector in time-gating mode (between 0.3 ns and 6 ns) to eliminate laser reflection. The whole system was driven by LAS X (Leica).

2.9. Mass spectrometry

Mass spectrometry measurements were performed with an electrospray Triple-TOF 4600 mass spectrometer (ABSciex) coupled to the nanoRSLC ultra performance liquid chromatography system (Thermo Scientific) equipped with a C4-desalting column. For ESI−MS measurements, the instrument was operated in positive and RF quadrupole modes with the TOF data being collected between m/z 400−2990. Collision energy was set to 10 eV and azote was used as collision gas. Mass spectra acquisition was performed after loading and desalting of protein samples on C4-column. The Analyst and Peakview softwares were used for acquisition and data processing, respectively. The protein average masses are calculated from the spectra with a mass accuracy of ±2 Da.

3. Results

3.1. Partial rescue of the respiratory defect of yeast bcs1-F401I mutant by ARTS

The yeast mutation *bcs1*-F401I is the equivalent of the human mutation *BCS1L*-F368I found in a patient with early-onset encephalopathy [33]. The yeast mutant is respiratory deficient and thus unable to grow on a non-fermentable medium containing glycerol as sole carbon source. When solid, non-fermentable medium was spread with a lawn of the mutant, a halo of growing cells appeared around the filters where ARTS was spotted, showing that this drug was able to partially restore the respiratory growth of the yeast mutant (Fig. 1A).

We next grew the *bcs1*-F401I mutant in liquid galactose medium containing various concentrations of ARTS (Fig. 1B). In this medium, yeast cells use both fermentation and respiration to proliferate. After 29 h of growth in drug-free medium, the *bcs1*-F401I mutant exhibited a significantly reduced growth compared to the wild type (wt) with an OD_{600} nearly three times lower (10 compared to 27). The addition of ARTS to the medium partially rescued the respiratory growth defect of the mutant, with the most effective ARTS concentrations ranging from 3 to 10 µM. For both the mutant and wt strains, high concentrations of ARTS inhibited growth, with the *bcs1* mutant being less sensitive to the drug and exhibiting an IC_{50} (drug concentration inhibiting the cell growth by 50%) of around 30 µM compared to 10 µM for the wt. In parallel, we found that addition of 5 µM ARTS for two days raised the oxygen (O_2) consumption of the mutant from about 15% to 50% of that of wt cells, showing that the respiratory capacity of the *bcs1* mutant significantly increased in presence of ARTS (Fig. 1C).

Finally, we have performed BN-PAGE followed by western blot on mitochondria purified from wt as well as *bcs1*-F401I cells grown with or without 5 µM ARTS (Fig.1D). Under our conditions, the anti-Cyt1 antibodies mainly detected the wt complex III in the form of supercomplexes III/IV. Conversely, in the mutant, inactive pre-complexes III that were previously shown to contain cytochrome *c1* but lack the catalytic subunit Rip1 [25-29]

accumulated. In the presence of ARTS, the steady state level of these pre-complexes III slightly decreased by about 30%. Immunodetection of the complex IV subunit Cox2 in the same samples revealed only supercomplexes III/IV in the wild type while in the *bcs1*-F401I mutant there appeared to be a whole range of illegitimate complexes IV, already described in *rip1* and *bcs1* mutants [29, 43, 44], that migrated from the position of pre-complexes III up to the position of the *bona fide* complex III/IV. Thus, using BN-PAGE, we could not confidently discriminate supercomplexes III/IV from the various illegitimate pre-III/IV present the *bcs1*-F401I mutant. Next, immunoprecipitation experiments of the early-assembled complex III subunit Qcr7 fused to a c-Myc tag retrieved Rip1 massively in the wild-type and only barely in the Bcs1-F401I mutant. However no increase of Rip1 level could be detected after ARTS treatment of the mutant, suggesting that the drug causes only very little, if any, increase in mature complex III level (see Fig. S1). Thus the oxygen uptake restoration upon ARTS treatment might be due either to a tiny increase of mature complex III too subtle to be detected in our experiments or to a decrease of pre-III or illegitimate pre-III/IV complexes, whose accumulation in the mutant is likely to alter respiration (see discussion).

3.2. ARTS affects the steady state level of respiratory complex cytochromes in yeast

As the complex III contains two cytochromes, cytochrome *b* and *c1*, and heme has been implicated as a key molecule activating ART (see introduction), we decided to determine the effect of ARTS on mitochondrial cytochromes in wt and mutant *bcs1* cells. The association of the apoproteins Cytb and Cyt1 with their heme cofactor to form cytochromes *b* and *c1* respectively is required at an early stage of complex III assembly. These two cytochromes, as well as cytochrome *c* and cytochrome *a+a3* from complex IV, once fully assembled and reduced, show specific light absorption maxima that can be monitored and quantified by recording cytochrome spectra from whole yeast cells (Fig. 2A). Wt and *bcs1*-F401I cells were

grown with increasing concentrations of ARTS and the cytochrome levels were quantified relative to the drug free control (Fig. 2B). For the wt at drug concentrations that did not affect cell growth under our conditions (*i.e.* 1 µM and 3 µM), the levels of cytochromes *b*, *c1* and *c* decreased by 30% to 40% with 1 µM ARTS and by 40% to 50% with 3 µM ARTS while cytochrome *a+a3* was less affected. Treatment of the wt with 10 µM ARTS, the drug concentration corresponding to the IC_{50}, led to a significant decrease of all cytochrome levels by at least 60%. For *bcs1*-F401I, the levels of cytochromes *b*, *c1* and *c* were only slightly decreased by treatment with 3 µM ARTS and lowered by 50 to 60% with 10 µM drug. Thus, ARTS treatment strongly lowers the absorption spectrum maxima of mitochondrial cytochromes, cytochromes *c, c1* and *b* being more affected than cytochrome *a+a3*.

We next determined whether the ARTS-induced decrease in cytochrome spectra was associated with a lower level of the corresponding apoprotein. Mitochondria from wt and *bcs1*-F401I cells grown with increasing concentrations of ARTS were purified. The steady state level of Cytb and Cyt1 of complex III, Cytc, and the complex IV subunit Cox1 which binds the hemes *a* and *a3* were analyzed by western blot (Fig. 2C). The results show that the steady state level of all mitochondrial cytochromes was reduced at high ARTS concentrations, starting from 3 µM ARTS for the wt and 10 µM for the mutant. With the anti-Cyt1 antibody, a band of lower mobility appeared first when wt or *bcs1*-F401I cells were grown with 1 µM or 10 µM ARTS respectively. In the wt, this lower mobility band became more intense when the concentration of ARTS increased. It is well known that yeast pre-Cyt1 is processed in two sequential steps [45, 46]. The first processing takes place in the mitochondrial matrix where the signal sequence addressing pre-Cyt1 to the mitochondria is removed to give the intermediate form of Cyt1 (i-Cyt1). Then heme *c1* has to be covalently attached to the apoprotein i-Cyt1 by heme lyase before allowing the second processing step to occur in the intermembrane space, thus generating mature cytochrome Cyt1 (Fig. S2A). Thus, in the yeast mutant deprived of heme

lyases (Δ*hl*), the i-Cyt1 accumulates. This i-Cyt1 band appeared to co-migrate with the lower mobility band generated in presence of ARTS in both the wt and *bcs1*-F401I. This suggests that ARTS treatment disturbs the second step of yeast pre-Cyt1 maturation. Taken together, the results in Fig. 2 show that ARTS treatment decreased the steady state levels of OXPHOS cytochromes, and that the *bcs1*-F401I mutant was less sensitive to this effect.

3.3. A fluorescent version of DHA targets cytochromes c and c1 in yeast mitochondria

In mammals, ART-derived drugs are *in vivo* prodrugs of DHA, which is mainly produced by the action of the liver isoenzyme 3A4 of cytochrome P450 [47-49]. For these reasons, their biological action is believed to recapitulate that of DHA ([50] and for review [1]). Thus, to investigate the compensation mechanisms by defining the targets of ART-derived drugs, we decided to use a fluorescent version of DHA, Fluo-DHA (Fig. 3A, Sissoko *et al*., submitted to ACS Infectious Diseases).

First, using the halo test, we showed that like for ARTS, the respiratory growth defect of the *bcs1*-F401I mutant was partially rescued by ART, DHA and Fluo-DHA (Fig. 3B). We found that the optimal rescuing concentrations in liquid cultures were around 1 µM for ART and DHA and 3 µM for Fluo-DHA (data not shown). Altogether these data indicate that Fluo-DHA is able to improve the respiratory growth of the *bcs1*-F401I mutant, thus validating its use as a fluorescent probe.

Second, to localize Fluo-DHA within live yeast, wt cells were incubated successively with MitoTracker®, a red-fluorescent dye that stains mitochondria, and with Fluo-DHA, before fluorescence imaging using a confocal microscope (Fig. 3C). We observed that Fluo-DHA rapidly labeled the yeast mitochondria (in less than 5 min) since it colocalized with MitoTracker®. Thus, we conducted *in organello* interaction experiments to identify the mitochondrial targets of Fluo-DHA. We incubated Fluo-DHA for 15 min with mitochondria purified from wt and mutants deprived of cytochrome *c1* (Δ*c1*), cytochrome *c* (Δ*c*) or heme

lyases (Δ*hl*). Mitochondrial proteins were then resolved by SDS-PAGE and visualized using gel fluorescence imaging and Western blot analysis (Fig. 3D). Two main fluorescent bands were detected in wt mitochondria upon incubation with Fluo-DHA, consistent with the formation of covalent protein adducts resistant to denaturing conditions. These two bands had the same migration profile than Cyt1 and Cytc. This was further confirmed since with mitochondria from Δ*c1* or Δ*c* only one band appeared, corresponding to the molecular weight of Cytc or Cyt1 respectively, moreover all fluorescent signal was lost in Δ*hl*, showing that Fluo-DHA does not interact with i-Cyt1 in absence of its heme moiety. Regardless of the strain tested, no fluorescent bands were detected at the size corresponding to Cytb and Cox1. This could be due to the non-covalent nature of the interactions existing between these apoproteins and their corresponding hemes, or to the fact that the heme moieties of Cytb and Cox1 are buried into the inner membrane, thereby preventing or delaying the activation and chemical attack by ART derivatives. Thus, Fluo-DHA appears to target *c*-type cytochromes in yeast mitochondria.

3.4. ART derivatives also primarily target human mitochondrial cytochromes c and c1

Since ART derivatives are used in clinics against the malaria parasite and have more recently been tested as a possible therapy for cancers (see Introduction), we investigated the mode of action of ARTS in human cells by testing if it also targeted mitochondrial *c*-type cytochromes. First, when adding Fluo-DHA to whole human cells we observed that it rapidly labeled mitochondria as shown by colocalization with MitoTracker® (Fig. 4A). Then, HEK293T human cells were grown for a week with different concentrations of ARTS and whole cell protein extracts were resolved by SDS-PAGE and analyzed by Western blot analysis (Fig. 4B). When ARTS concentration increased, the abundance of mature cytochrome *c1* decreased while a lower mobility band appeared, consistent with the accumulation of partially processed cytochrome *c1*. The sequence comparison between the yeast Cyt1 and human CYC1 shows a

good conservation of (i) the hydrophobic stretch important for the processing and insertion of yeast Cyt1 and (ii) the position of the proteolytic processing site generating the mature cytochrome *c1* between yeast and human cells (Fig. S2B). Thus it is tempting to speculate that the processing steps are conserved. In yeast, heme is required for the second step of processing [45, 46] and our results suggest that heme is also probably required for the processing of human CYC1. Similarly, the cytochrome *c* signal tended to decrease as the drug concentration increased. Thus, ARTS treatment appears to interfere with the maturation of cytochrome *c1* and the stability of cytochrome *c* in human cells.

To investigate the molecular targets of ART derivatives in humans, *in organello* and whole cell interaction experiments were conducted (Fig. 4C). Purified human mitochondria were incubated for 15 min and whole cells were incubated for 3 h with Fluo-DHA, proteins were extracted and analyzed. In presence of Fluo-DHA, two main bands appeared at the size corresponding to cytochromes *c1* and *c* in both the mitochondrial and total protein samples in presence of Fluo-DHA, implying the formation of covalent adducts between DHA and the cytochromes. The fact that total proteins exhibited the same fluorescence profile as mitochondrial proteins strongly suggests that mitochondrial *c*-type cytochromes are protein targets of Fluo-DHA in human cells.

3.5. Fluo-DHA selectively interacts with reduced cytochrome c

To analyze the mechanism of interaction between Fluo-DHA and cytochrome *c*, we incubated purified cytochrome *c* from equine heart with Fluo-DHA under various conditions and ran SDS-PAGE gels to resolve Fluo-DHA and cytochrome *c* (Fig. 5A).

Beforehand we determined by recording its 550 nm absorption that 65% of the purified cytochrome *c* was in its oxidized form. This purified cytochrome *c* spontaneously presented a low level of fluorescence, that doubled upon a 15 min incubation with Fluo-DHA. Upon full

oxidation of cytochrome *c* by a pre-incubation with H_2O_2, the intrinsic fluorescence signal of cytochrome *c* became barely detectable, independently of the addition of Fluo-DHA, suggesting that the reduction state of cytochrome *c* was critical for its interaction with Fluo-DHA. When the purified cytochrome *c* was fully reduced prior to incubation with Fluo-DHA, the fluorescence signal increased about four times, and up to five times when the loading buffer was supplemented with the reducing agent DTT. This was likely explained by the capability of DTT to maintain a fully reduced cytochrome *c* (of which a small proportion otherwise undergoes re-oxidation during sample preparation) allowing continuation of its reaction with Fluo-DHA in the loading buffer. As controls, we showed that (i) pre-incubating reduced cytochrome *c* with excess DHA decreased the subsequent binding of Fluo-DHA by about 30%, indicating that DHA and Fluo-DHA competed for identical binding site(s) on cytochrome *c*, and (ii) increasing the concentration of Fluo-DHA enhanced the fluorescence signal in a dose-response manner (Fig. 5B). Taken together, our results show that Fluo-DHA selectively interacts with reduced cytochrome *c*.

3.6. Characterization of DHA covalent binding to the heme of reduced cytochrome c

The mechanism of free heme alkylation by ART upon reductive cleavage of its endoperoxide pharmacophore has been precisely described [51-54] and found to be a common feature of endoperoxide-containing antimalarial drugs [55, 56]. Based on our observation of stable adducts between Fluo-DHA and reduced cytochrome *c* in SDS-PAGE, we performed electrospray ionization mass spectrometry to test if a covalent reaction could be definitely established between cytochrome *c* and DHA.

Fully-reduced cytochrome *c* was incubated for 15 min with increasing amounts of DHA and submitted to mass spectrometry analysis (Fig. 6). The molecular masses of the experimentally detected species were compared to the predicted ones (Fig. S3). When reduced

cytochrome *c* was incubated with DMSO only, a main peak compatible with the predicted mass was observed, together with a minor peak corresponding to a form with a methionine oxidation (Fig. 6, upper panels, and Table S1). In presence of increasing amounts of DHA, three new peaks appeared (Fig. 6, bottom panels). The peak at *m/15z* ~ 843.8 corresponded to the predicted value for covalent DHA-cytochrome *c* adduct. The peak at about *m/15z* ~ 839.8 was consistent with a rearranged product following C-alkylation of cytochrome *c* by DHA and loss of an acetate fragment. The peak at about *m/15z* 841.0 likely corresponded to the same species than the *m/15z* 839.8 but with a methionine-oxidized form of the cytochrome *c*. The total relative abundance of all DHA-cytochrome *c* adducts tended to increase with the amount of DHA added, to reach 20% of bio-incorporation of DHA into cytochrome *c* at a 10:1 ratio (Table S1). No difference in the DHA incorporation could be observed when increasing the incubation time (from 15 min to 60 min, data not shown) indicating that cytochrome *c* alkylation by DHA was a very fast process, in accordance with our *in vitro* and *in cellulo* data. Altogether, these results strongly suggest that the porphyrin rings of hemes rather than the apoproteins are the actual sites of alkylation by ART derivatives at the level of yeast and mammalian mitochondrial *c*-type cytochromes.

4. Discussion-conclusion

In this work, we combined the use of *in cellulo*, *in organello* and *in vitro* analyses to gain insights into the molecular targets and biological effects of ART and its derivatives, in yeast and human mitochondria. All the data that we gathered by these different approaches are fully consistent with an interaction of ART derivatives with mitochondrial cytochromes that are catalytic components of the respiratory chain, and particularly with *c*-type cytochromes. The effect of ART derivatives on yeast cytochromes *b* and *a+a3* might be either the result of the direct binding of artemisinins to these cytochromes or a secondary effect of the loss of

mature cytochromes *c* and *c1*. Indeed, it is well known that the steady state levels of Cytb and Cox subunits closely depend on that of Cyt1 and Cytc respectively (*e.g.* [57, 58]).

Low concentrations of ART and its derivatives are able to phenotypically rescue a respiration-defective yeast mutant harboring a mutation in the Bcs1 protein, a key chaperone in mitochondrial complex III assembly. The interference of ART derivatives with the maturation of the complex III subunit cytochrome *c1* might directly explain this compensatory effect. Assembly of complex III is indeed delayed in the *bcs1*-F401I yeast mutant and a large amount of inactive cytochrome *c1*-containing pre-complex III accumulates. This is deleterious because complex IV is trapped in an inactive preIII/IV supercomplex [29]; in addition, this pre-complex III that accumulates in the inner-membrane could also be toxic by itself. Thus, it is likely that decreasing the quantity of complex IV [29] or mature cytochrome *c1* (this work) limits the accumulation of pre-complex III and frees some complex IV, which can then associate with the small amount of complex III that slowly assembles despite the *bcs1*-F401I mutation. Together, this could restore some respiratory growth thanks to a very subtle equilibrium taking place between the rate of assembly of individual complexes and supercomplex association. Interestingly, the complex III deficiency due to the corresponding *BCS1L* mutation in the patient muscle or liver is also associated with the accumulation of a cytochrome *c1*-containing pre-complex III [33], thus it would be highly relevant in the future to test whether ARTS might also decrease the accumulation of this aberrant pre-complex in patient cells and improve their respiratory capacity.

In order to be a direct target of Fluo-DHA *in vitro*, purified cytochrome *c* is required to be under its reduced form. This observation is fully consistent with the fact that ART and its derivatives require reduced forms of iron (mainly heme from hemoglobin digestion in the malaria parasites) to become bioactivated under the form of protein-reactive radicals [3-8]. The need of a reduced metal might also account for the limited sensitivity to ART and ARTS

displayed by the respiratory-deficient *bcs1*-F401I cells (this paper) or other yeast respiratory mutants [9, 12] compared to the wt since the reduction kinetics of cytochromes is slower in respiratory deficient mutants. Similarly, HeLa cells were previously shown to be less sensitive to ARTS when they are *rho*^{0}, *i.e.* devoid of an active respiratory chain [15]. In conclusion, we propose that reduced cytochromes *per se* might activate ART and its derivatives in mitochondria.

In the malaria parasite, using ART-based profiling probes, a hundred of ART covalent binding protein targets were identified upon heme activation [5, 7]. These protein targets of ART belong to multiple metabolic pathways, but no enrichment in cytochromes were found. This strikingly contrasts with our yeast and human cell data showing only a few dominant and specific protein targets (*c*-type cytochromes). This apparent discrepancy could be explained by the dramatically different sources and abundance of cellular heme between species, which in malaria parasites are constituted mainly by hemoglobin digestion products. Whether plasmodial *c*-type cytochromes are targeted by ART and participate to its antimalarial mode of action remains to be investigated knowing that a number of effective drugs target the parasite mitochondria (for review [59]).

In addition, ART and its derivatives are also active in cancer cells, mostly *via* arrest of cell cycle or apoptosis. The general oxidative stress appears to play a central role in these processes. We propose that the decrease in membrane potential and increase of mitochondrial ROS production already described in yeast and human cancer cells upon ARTS treatment might be direct consequences of the effect on mitochondrial cytochromes that we uncovered in this work. In cancer cells, this effect might be further enhanced by an increase of heme and lysosomal iron contents that could also be a source of ROS, thus synergistic pathways where iron (II)-containing molecules play a central role might contribute to the anti-cancer activity of ART and its derivatives.

Declaration of competing interest

No conflict of interest.

Acknowledgements

We thank Laure Crabbe, Francesca Giordano, Pierrick Le Borgne and Anne-Marie Tassin for useful technical advices and the members of the MITOSCREEN consortium for fruitful discussions. We are grateful to Christopher J. Herbert for critical reading of the manuscript and for looking over the English. The present work has benefited from the light microscopy facility of Imagerie-Gif, member of IBiSA and supported by "France-BioImaging" and the Labex "Saclay Plant Sciences". We thank Laëtitia Besse and Romain Le Bars for their advice and help for the experiments and the presentation of the results. This work has benefited from the facilities and expertise of the I2BC proteomic platform SICaPS, supported by IBiSA, Ile de France Region, Plan Cancer, CNRS and Paris-Sud University. We thank Virginie Redeker for a fruitful initial discussion about mass spectrometry analyses.

This work as well as AB and AL were supported by a grant from the "Association Française contre les Myopathies" (AFM, N°17122) within the MITOSCREEN consortium. DT-T was supported by a post-doctoral grant from the "Fondation pour la Recherche Médicale" (FRM N°DRM201001220457). JO was a PhD student from the University Evry-Val d'Essonne and was the recipient of a fellowship from the Ministère de la Recherche et de la Technologie.

References

[1] W.E. Ho, H.Y. Peh, T.K. Chan, W.S.F. Wong, Artemisinins: Pharmacological actions beyond anti-malarial, *Pharmacol. & Ther.* **142** (2014) 126–139.

[2] S. Bhatt, D.J. Weiss, E. Cameron, D. Bisanzio, B. Mappin, U. Dalrymple, K. Battle, C.L. Moyes, A. Henry, P.A. Eckhoff, E.A. Wenger, O. Briët, M.A. Penny, T.A. Smith, A. Bennett, J. Yukich, T.P. Eisele, J.T. Griffin, C.A. Fergus, M. Lynch, F. Lindgren, J.M. Cohen, C.L.J. Murray, D.L. Smith, S.I. Hay, R.E. Cibulskis, P.W. Gething, The effect of malaria control on *Plasmodium falciparum* in Africa between 2000 and 2015, *Nature* **526** (2015) 207–211.

[3] Y.Z. Yang, B. Little, S.R. Meshnick, Alkylation of proteins by artemisinin. Effects of heme, pH, and drug structure, *Biochem. Pharmacol.* **48** (1994) 569–573.

[4] B. Meunier, A. Robert, Heme as trigger and target for trioxane-containing antimalarial drugs, *Acc. Chem. Res.* **43** (2010) 1444–1451.

[5] J. Wang, C.J. Zhang, W.N. Chia, C.C. Loh, Z. Li, Y.M. Lee, Y. He, L.X. Yuan, T.K. Lim, M. Liu, C.X. Liew, Y.Q. Lee, J. Zhang, N. Lu, C.T. Lim, Z.C. Hua, B. Liu, H.M. Shen, K.S. Tan, Q. Lin, Haem-activated promiscuous targeting of artemisinin in P*lasmodium falciparum*, *Nat. Commun.* **6** (2015) 10111.

[6] L. Tilley, J. Straimer, N.F. Gnädig, S.A. Ralph, D.A. Fidock, Artemisinin action and resistance in *Plasmodium falciparum*, *Trends Parasitol.* **32** (2016) 682–696.

[7] H.M. Ismail, V. Barton, M. Phanchana, S. Charoensutthivarakul, M.H. Wong, J. Hemingway, G.A. Biagini, P.M. O'Neill, S.A. Ward, Artemisinin activity-based probes identify multiple molecular targets within the asexual stage of the malaria parasites *Plasmodium falciparum* 3D7, *Proc. Natl Acad. Sci. USA* **113** (2016) 2080–2085.

[8] J.L. Bridgford, S.C. Xie, S.A. Cobbold, C.F.A. Pasaje, S. Herrmann, T. Yang, D.L. Gillett, L.R. Dick, S.A. Ralph, C. Dogovski, N.J. Spillman, L. Tilley, Artemisinin kills malaria parasites by damaging proteins and inhibiting the proteasome, *Nat. Commun.* **9** (2018) 3801.

[9] W. Li, W. Mo, D. Shen, L. Sun, J. Wang, S. Lu, J.M. Gitschier, B. Zhou, Yeast model uncovers dual roles of mitochondria in action of artemisinin, *PLoS Genet.* **1** (2005) e36.

[10] J. Wang, L. Huang, J. Li, Q. Fan, Y. Long, Y. Li, B. Zhou, Artemisinin directly targets malarial mitochondria through its specific mitochondrial activation, *PLoS One* **5** (2010) e9582.

[11] T. Antoine, N. Fisher, R. Amewu, P.M. O'Neill, S.A. Ward, G.A. Biagini, Rapid kill of malaria parasites by artemisinin and semi-synthetic endoperoxides involves ROS-dependent depolarization of the membrane potential, *J. Antimicrob. Chemother.* **69** (2014) 1005–1016.

[12] C. Sun, B. Zhou, The molecular and cellular action properties of artemisinins: what has yeast told us? *Microbial Cell* **3** (2016) 196–205.

[13] S. Zhang, G.S. Gerhard, Heme mediates cytotoxicity from artemisinin and serves as a general anti-proliferation target, *PLoS One* **4** (2009) e7472.

[14] J. Zhang, X. Sun, L. Wang, Y.K. Wong, Y.M. Lee, C. Zhou, G. Wu, T. Zhao, L. Yang, L. Lu, J. Zhong, D. Huang, J. Wang, Artesunate-induced mitophagy alters cellular redox status, *Redox Biol.* **19** (2018) 263–273.

[15] A.E. Mercer, I.M. Copple, J.L. Maggs, P.M. O'Neill, B.K. Park, The role of heme and the mitochondrion in the chemical and molecular mechanisms of mammalian cell death induced by the artemisinin antimalarials, *J. Biol. Chem.* **286** (2011) 987–996.

[16] A. Hamacher-Brady, S.H. Tan, S. Ng, Y. Shi, J. Zhou, K.S. Tan, W.S. Wong, H.M. Shen, Artesunate activates mitochondrial apoptosis in breast cancer cells via iron-catalyzed lysosomal reactive oxygen species production, *J. Biol. Chem.* **286** (2011) 6587–6601.

[17] N.D. Yang, S.H. Tan, S. Ng, Y. Shi, J. Zhou, K.S. Tan, W.S. Wong, H.M. Shen, Artesunate induces cell death in human cancer cells via enhancing lysosomal function and lysosomal degradation of ferritin, *J. Biol. Chem.* **289** (2014) 33425–33441.

[18] J. Wang, J. Zhang, Y. Shi, C. Xu, C. Zhang, Y.K. Wong, Y.M. Lee, S. Krishna, Y. He, T.K. Lim, W. Sim, Z.C. Hua, H.M. Shen, Q. Lin, Mechanistic investigation of the specific anticancer property of artemisinin and its combination with aminolevulinic acid for enhanced anticolorectal cancer activity, *ACS Cent. Sci.* **3** (2017) 743–750.

[19] A. Bhaw-Luximon, D. Jhurry, Artemisinin and its derivatives in cancer therapy: status of progress, mechanism of action, and future perspectives, *Cancer Chemother. Pharmacol.* **79** (2017) 451–466.

[20] Y.F. Dai, W.W Zhou, J. Meng, X.L. Du, Y.P. Sui, L. Dai, P.Q. Wang, H.R. Huo, F. Sui, The pharmacological activities and mechanisms of artemisinin and its derivatives: a systematic review, *Med. Chem. Res.* **26** (2017) 867–880.

[21] E. Konstat-Korzenny, J. Ascencio-Aragón, S. Niezen-Lugo, R. Vázquez-López, Artemisinin and its synthetic derivatives as a possible therapy for cancer, *Med. Sci.* **6** (2018) 19.

[22] H.J. Kim, O. Khalimonchuk, P.M. Smith, D.R. Winge, Structure, function, and assembly of heme centers in mitochondrial respiratory complexes, *Biochim. Biophys. Acta* **1823** (2012) 1604–1616.

[23] P. Hamel, V. Corvest, P. Giegé, G. Bonnard, Biochemical requirements for the maturation of mitochondrial *c*-type cytochromes, *Biochim. Biophys. Acta* **1793** (2009) 125–138.

[24] P.M. Smith, J.L. Fox, D.R. Winge, Biogenesis of the cytochrome *bc(1)* complex and role of assembly factors, *Biochim. Biophys. Acta* **1817** (2012) 276–286.

[25] F.G. Nobrega, M.P. Nobrega, A. Tzagoloff, *BCS1*, a novel gene required for the expression of functional Rieske iron-sulfur protein in *Saccharomyces cerevisiae*, *EMBO J.* **11** (1992) 3821–3829.

[26] C.M. Cruciat, K. Hell, H. Fölsch, W. Neupert, R.A. Stuart, Bcs1p, an AAA-family member, is a chaperone for the assembly of the cytochrome *bc1* complex, *EMBO J.* **18** (1999) 5226–5233.

[27] L. Conte, B.L. Trumpower, V. Zara, Bcs1p can rescue a large and productive cytochrome *bc1* complex assembly intermediate in the inner membrane of yeast mitochondria, *Biochim. Biophys. Acta* **1813** (2011) 91–101.

[28] N. Wagener, M. Ackermann, S. Funes, W. Neupert, A pathway of protein translocation in mitochondria mediated by the AAA-ATPase Bcs1, *Mol. Cell* **44** (2011) 191–202.

[29] J. Ostojić, C. Panozzo, J.P. Lasserre, C. Nouet, F. Courtin, C. Blancard, J.P. di Rago, G. Dujardin, The energetic state of mitochondria modulates complex III biogenesis through the ATP-dependent activity of Bcs1, *Cell Metab.* **18** (2013) 567–577.

[30] P. de Lonlay, I. Valnot, A. Barrientos, M. Gorbatyuk, A. Tzagoloff, J.W. Taanman, E. Benayoun, D. Chrétien, N. Kadhom, A. Lombès, H.O. de Baulny, P. Niaudet, A. Munnich, P. Rustin, A. Rötig, A mutant mitochondrial respiratory chain assembly protein causes complex III deficiency in patients with tubulopathy, encephalopathy and liver failure, *Nat. Genet.* **29** (2001) 57–60.

[31] I. Visapää, V. Fellman, J. Vesa, A. Dasvarma, J.L. Hutton, V. Kumar, G.S. Payne, M. Makarow, R. Van Coster, R.W. Taylor, D.M. Turnbull, A. Suomalainen, L. Peltonen, GRACILE syndrome, a lethal metabolic disorder with iron overload, is caused by a point mutation in *BCS1L*, *Am. J. Hum. Genet.* **71** (2002) 863–876.

[32] J.T. Hinson, V.R. Fantin, J. Schönberger, N. Breivik, G. Siem, B. McDonough, P. Sharma, I. Keogh, R. Godinho, F. Santos, A. Esparza, Y. Nicolau, E. Selvaag, B.H. Cohen, C.L. Hoppel, L. Tranebjaerg, R.D. Eavey, J.G. Seidman, C.E. Seidman, Missense mutations in the *BCS1L* gene as a cause of the Björnstad syndrome, *N. Engl. J. Med.* **356** (2007) 809–819.

[33] E. Fernandez-Vizarra, M. Bugiani, P. Goffrini, F. Carrara, L. Farina, E. Procopio, A. Donati, G. Uziel, I. Ferrero, M. Zeviani, Impaired complex III assembly associated with *BCS1L* gene mutations in isolated mitochondrial encephalopathy, *Hum. Mol. Genet.* **16** (2007) 1241–1252.

[34] M. Morán, L. Marín-Buera, M.C. Gil-Borlado, H. Rivera, A. Blázquez, S. Seneca, M. Vázquez-López, J. Arenas, M.A. Martín, C. Ugalde, Cellular pathophysiological consequences

of *BCS1L* mutations in mitochondrial complex III enzyme deficiency, *Hum. Mutat.* **31** (2010) 930–941.

[35] R. A. Baker, J.R.C. Priestley, A.M. Wilstermann, K.J. Reese, P.R. Mark , Clinical spectrum of BCS1L Mitopathies and their underlying structural relationships, AMM. J. Med. Genet. A. **179** (2019) 373-380

[36] M. Oláhová, C.C. Berti, J.J. Collier, C.L. Alston, E. Jameson, S.A. Jones, N. Edwards, L. He, P.F. Chinnery, R. Horvath, P. Goffrini, R.W. Taylor, J.A. Sayer, Molecular genetic investigations identify new clinical phenotypes associated with BCS1L-related mitochondrial disease, Hum Mol Genet. **28** (2019) 3766-3776.

[37] C. Panozzo, A. Laleve, D. Tribouillard-Tanvier, J. Ostojić, C.H. Sellem, G. Friocourt, A. Bourand-Plantefol, A. Burg, A. Delahodde, M. Blondel, G. Dujardin, Chemicals or mutations that target mitochondrial translation can rescue the respiratory deficiency of yeast *bcs1* mutants, *Biochim. Biophys. Acta* **1864** (2017) 2297–2307.

[38] G. Dujardin, P. Pajot, O. Groudinsky, P.P. Slonimski, Long range control circuits within mitochondria and between nucleus and mitochondria. I. Methodology and phenomenology of suppressors, *Mol. Gen. Genet.* **179** (1980) 469–482.

[39] E. Couplan, R.S. Aiyar, R. Kucharczyk, A. Kabala, N. Ezkurdia, J. Gagneur, R.P. St Onge, B. Salin, F. Soubigou, M. Le Cann, L.M. Steinmetz, J.P. di Rago, M. Blondel, A yeast-based assay identifies drugs active against human mitochondrial disorders, *Proc. Natl Acad. Sci. USA* **108** (2011) 11989–11994.

[40] Y. Saint-Georges, N. Bonnefoy, J.P. di Rago, S. Chiron, G. Dujardin, A pathogenic cytochrome *b* mutation reveals new interactions between subunits of the mitochondrial *bc1* complex, *J. Biol. Chem.* **277** (2002) 49397–49402.

[41] C. Lemaire, G. Dujardin, "Preparation of respiratory chain complexes from *Saccharomyces cerevisiae* wild-type and mutant mitochondria" in *Organelle Proteomics*, D. Pflieger, J. Rossier, Eds. (Humana Press, 2008) **432**, pp. 65–81.

[42] A.J. Johnston, J. Hoogenraad, D.A. Dougan, K.N. Truscott, M. Yano, M. Mori, N.J. Hoogenraad, M.T. Ryan, Insertion and assembly of human TOM7 into the preprotein translocase complex of the outer mitochondrial membrane, *J. Biol. Chem.* **277** (2002) 42197–42204.

[43] C.M. Cruciat, S. Brunner, F. Baumann, W. Neupert, R.A. Stuart, The cytochrome bc1 and cytochrome c oxidase complexes associate to form a single supracomplex in yeast mitochondria, J. Biol. Chem. **275** (2000) 18093-18098.

[44] T.Z. Cui, A. Comte, J.L. Fox, V. Zara, D.R. Winge , Modulation of the respiratory supercomplexes in yeast: enhanced formation of cytochrome oxidase increases the stability and abundance of respiratory supercomplexes, J. Biol. Chem. **289** (2014) 6133-6141.

[45] D.W. Nicholson, R.A. Stuart, W. Neupert, Biogenesis of cytochrome *c1*. Role of cytochrome *c1* heme lyase and of the two proteolytic processing steps during import into mitochondria, *J. Biol. Chem.* **264** (1989) 10156–10168.

[46] I. Arnold, H. Fölsch, W. Neupert, R.A. Stuart, Two distinct and independent mitochondrial targeting signals function in the sorting of an inner membrane protein, cytochrome *c1*, *J. Biol. Chem.* **273** (1998) 1469–1476.

[47] J.M. Grace, A.J. Aguilar, K.M. Trotman, J.O. Peggins, T.G. Brewer, Metabolism of beta-arteether to dihydroqinghaosu by human liver microsomes and recombinant cytochrome P450, *Drug Metab. Dispos.* **26** (1998) 313–317.

[48] K. Silamut, P.N. Newton, P. Teja-Isavadharm, Y. Suputtamongkol, D. Siriyanonda, M. Rasameesoraj, S. Pukrittayakamee, N.J. White, Artemether bioavailability after oral or

intramuscular administration in uncomplicated *falciparum* malaria, *Antimicrob. Agents Chemother.* **47** (2003) 3795–3798.

[49] R.K. Haynes, B. Fugmann, J. Stetter, K. Rieckmann, H.D. Heilmann, H.W. Chan, M.K. Cheung, W.L. Lam, H.N. Wong, S.L. Croft, L. Vivas, L. Rattray, L. Stewart, W. Peters, B.L. Robinson, M.D. Edstein, B. Kotecka, D.E. Kyle, B. Beckermann, M. Gerisch, M. Radtke, G. Schmuck, W. Steinke, U. Wollborn, K. Schmeer, A. Römer A, Artemisone, a highly active antimalarial drug of the artemisinin class, *Angew. Chem. Int. Ed. Engl.* **45** (2006) 2082–2088.

[50] V. Melendez, J.O. Peggins, T.G. Brewer, A.D. Theoharides, Determination of the antimalarial arteether and its deethylated metabolite dihydroartemisinin in plasma by high-performance liquid chromatography with reductive electrochemical detection, *J. Pharm. Sci.* **80** (1991) 132–138.

[51] A. Robert, B. Meunier, Characterization of the first covalent adduct between artemisinin and a heme model, *J. Am. Chem. Soc.* **119** (1997) 5968-5969.

[52] A. Robert, J. Cazelles, B. Meunier, Characterization of the alkylation product of heme by the antimalarial drug artemisinin, *Angew. Chem. Int. Ed. Engl.* **40** (2001) 1954-1957.

[53] A. Robert, F. Benoit-Vical, C. Claparols, B. Meunier, The antimalarial drug artemisinin alkylates heme in infected mice, *Proc. Natl Acad. Sci. USA* **102** (2005) 13676-13680.

[54] A. Accardo, S.A. Laurent, H. Mazarguil, M. Meyer, A. Robert, B. Meunier, Interaction of iron(II)-heme and artemisinin with a peptide mimic of *Plasmodium falciparum* HRP-II, *J. Inorg. Biochem.* **101** (2007) 1739-1747.

[55] S.A.L. Laurent, A. Robert, B. Meunier, C10-modified artemisinin derivatives: Efficient heme-alkylating agents, *Angew. Chem. Int. Ed. Engl.* **44** (2005) 2060-2063.

[56] F.B.E. Garah, B. Meunier, A. Robert, The antimalarial artemisone is an efficient heme alkylating agent, *Eur. J. Inorg. Chem*. **13** (2008) 2133-2135.

[57] M.D. Crivellone, M.A. Wu, A. Tzagoloff, Assembly of the mitochondrial membrane system. Analysis of structural mutants of the yeast coenzyme QH2-cytochrome c reductase complex, *J. Biol. Chem.* **263** (1988) 14323-14333.

[58] D.A. Pearce, F. Sherman, Degradation of cytochrome oxidase subunits in mutants of yeast lacking cytochrome *c* and suppression of the degradation by mutation of *yme1, J. Biol. Chem.* **270** (1995) 20879-20882.

[59] C.D. Goodman, H.D. Buchanan, G.I. McFadden, Is the mitochondrion a good malaria drug target? *Trends Parasitol.* **33** (2017) 185–193.

Figure legends

Fig. 1. ARTS treatment compensates for the respiratory deficiency of the yeast *bcs1*-F401I mutant.

Panel A: The *bcs1*-F401I mutant was spread onto solid respiratory medium, then sterile filters were placed on the agar surface and loaded with 5 µl of either 1mM ARTS or DMSO only. The plates were incubated for a week at 28 °C.

Panel B: wt or *bcs1*-F401I cells were grown in liquid galactose medium, supplemented with or without 1, 2, 4, 8, 16, 32, 64 or 128 µM ARTS. The cell density was measured after a 29h growth. Data represent the mean ± SEM of at least three independent experiments. IC_{50} was estimated from the plot of cell density *vs* ARTS concentrations.

Panel C: O_2 consumption of wt and *bcs1*-F401I cells grown with 5 µM ARTS or DMSO only. Data represent the mean ± SEM of at least three independent experiments with at least three measurements per experiment.

Panel D: Mitochondrial proteins from wt and *bcs1*-F401I cells harboring a Qcr7-c-Myc tag [29], grown with 5 µM ARTS or DMSO, were purified and solubilized with digitonin. Several BN-PAGE were performed in parallel using the same solubilization extracts and transferred onto membranes that were immunoblotted with antibodies against Cyt1 or Cox2 to reveal complex III or IV respectively, as well as against Atp1 (complex V) as control. The positions of the different complexes, super-complexes and protein molecular mass markers (in kDa) are indicated. The steady state level of pre-complexes III revealed with the anti-Cyt1 antibodies that accumulated in the *bcs1*-F401I mutant repetitively decreased by about 30% (mean 33 ± 9) when the mutant is treated with ARTS.

.

Fig. 2. ARTS decreases the steady-state level of mitochondrial cytochromes.

Panel A: Examples of cytochrome absorption spectra of wt cells grown with 5 µM ARTS or

DMSO only: cytochrome *c* (*c*), cytochromes *c1* (*c1*) and *b* (*b*) from complex III and cytochromes *a*+*a3* (*aa3*) from complex IV.

Panel B: The absorption maxima for the four mitochondrial cytochromes were measured as in [35] from wt (top panel) or *bcs1*-F401I (bottom panel) cells grown without or with 1, 3, or 10 µM ARTS. Data are represented as the mean ± SEM of three experiments.

Panel C: Mitochondrial proteins were purified from wt and *bcs1*-F401I cells grown without or with 1, 3, or 10 µM ARTS and from the heme lyase deficient mutant (*Δhl*). They were analyzed by SDS-PAGE and immunoblotted with antibodies against Cyt1, Cytb, Cytc, Cox1 and Nam1 as a loading control. i-Cyt1 is a partially processed form of Cyt1.

Fig. 3. Fluo-DHA rapidly enters yeast mitochondria where it binds cytochromes *c* and *c1*.

Panel A: Chemical structure of Fluo-DHA**.**

Panel B: Compensation of the respiratory deficiency of the *bcs1*-F401I mutant by ART derivatives (as in Fig 1A).

Panel C: Fluorescence imaging of live yeast cells after a 20 min incubation with 3 µM Fluo-DHA and MitoTracker®. The scale bar corresponds to 5 µm.

Panel D: Mitochondrial proteins were purified from wt or mutants devoid of either heme lyases (Δ*hl*), cytochrome *c* (*Δc*) or cytochrome *c1* (*Δc1*). They were incubated with either 30 µM of Fluo-DHA, ARTS or DMSO only for 15 min and resolved by SDS-PAGE. Top panel: fluorescence imaging; reduced cytochrome *c* and *c1* present a low level of auto-fluorescence. Bottom panel: western blot using antibodies against yeast Cyt1, Cytc and Nam1 as a loading control.

Fig. 4. ARTS and Fluo-DHA target mitochondrial cytochromes *c* and *c1* in human cells.

Panel A: Fluorescence imaging of fixed HEK293T human cells after incubation with 5 µM Fluo-DHA and MitoTracker®. The scale bar corresponds to 10 µm.

Panel B: Western blot analysis of total proteins from human HEK293T cells grown with with or without 1, 3, 6 or 9 µM ARTS using antibodies against human cytochrome *c1 (*CYC1), cytochrome *c* (CYCS) and tubulin as a loading control.

Panel C: Fluorescence imaging and western blot analysis of purified human mitochondria incubated with or without 30µM Fluo-DHA for 15 min (left panel) or of total extract of HEK293T cells incubated without or with 10µM Fluo-DHA for 3 h (right panel). TOM40 and Tubulin were used as loading controls.

Fig. 5. Fluo-DHA binds purified reduced cytochrome *c*.

Panel A: 8 µM of equine cytochrome *c* were incubated, either directly or after reduction with ascorbate, without or with 6 µM Fluo-DHA, 8.8 mM H_20_2 or 12.5 mM DTT as indicated. Panel B: 8 µM of reduced equine cytochrome *c* were incubated either with non-fluorescent DHA prior to addition of Fluo-DHA (left), or with increasing amount of Fluo-DHA (right).

In both panels, the fluorescence intensity is presented in the histograms as a percentage of the control value with cytochrome *c* only. Under our conditions of detection, cytochrome *c* spontaneously presents a low level of intrinsic fluorescence that depends on its oxidative state.

Fig. 6. Mass spectrometry analysis of DHA-cytochrome *c* adducts.

8 µM reduced equine cytochrome *c* were incubated for 15 min without (DHA 0) or with increasing amount of DHA (20, 40, 80 µM) in presence of 12.5 mM DTT and analyzed by mass spectrometry after electrospray ionization. The two top panels represent the mass to charge ratio with an ionization of 15 and 14 for incubations without or with 20 µM DHA. In addition to the expected peaks corresponding to cytochrome *c*, additional peaks corresponding the predicted

mass of Cyt*c*-DHA adducts are detected in presence of DHA. The four bottom panels represent a magnification of the region of Cyt*c*-DHA adducts for increasing concentrations of DHA (see Fig. S3 for formula and Table S1 for quantifications). Arrows on the y axes correspond to the threshold of peak annotation.

Author contributions

AL both performed the experiments and analyzed the data to determine active/toxic doses, measure O_2 consumption, record cytochrome spectra and study in gel interaction between cytochromes and Fluo-DHA, with the help of AB-P for O_2 consumption measurements, mitochondrial preparations and western blots. CP constructed the yeast mutant strains and performed the microscopy experiments. IK purified the human mitochondria and brought her expertise in human cell culture and mitochondrial proteins. JO, AB-P and AB participated to the initial experiments following the drug screening. DC performed mass spectrometry analyses. BM brought her expertise in the modeling in yeast of anti-malaria drug, NB in mitochondrial biogenesis and JC in malaria. GD designed the experiments and participated to the analysis of data. DT-T and MB designed and performed the initial drug screening. AS synthesized the Fluo-DHA probe needed for these experiments under the supervision of RD. AL, GD, NB, RD wrote the initial draft and made revisions after the comments of the other authors.

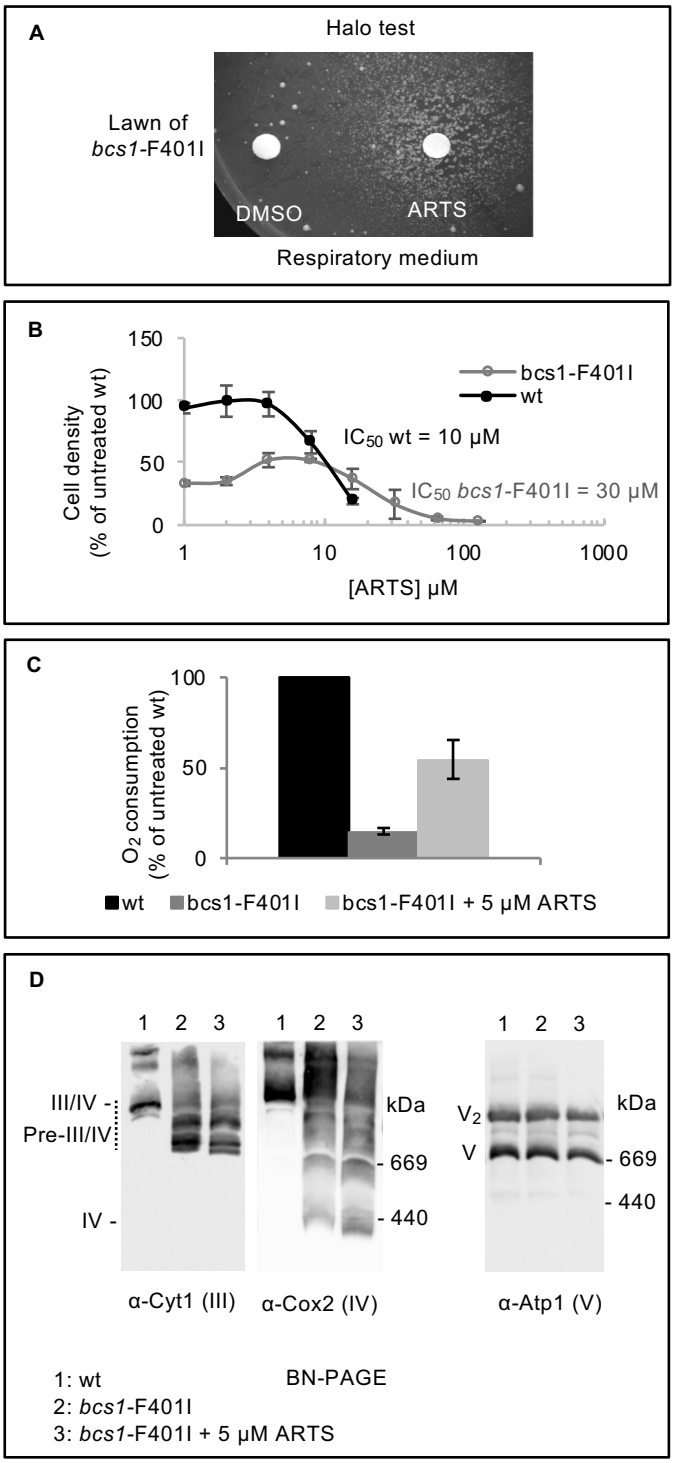
A
Halo test
Lawn of
bcs1-F401I
DMSO
ARTS
Respiratory medium
B
150
100
50
0
Cell density
(% of untreated wt)
bcs1-F401I
wt
IC50 wt = 10 µM
IC50 bcs1-F401I = 30 µM
1
10
100
1000
[ARTS] µM
C
100
50
0
O2 consumption
(% of untreated wt)
wt
bcs1-F401I
bcs1-F401I + 5 µM ARTS
D
1 2 3
1 2 3
1 2 3
III/IV -
Pre-III/IV
IV -
kDa
- 669
- 440
V2
V
kDa
- 669
- 440
α-Cyt1 (III)
α-Cox2 (IV)
α-Atp1 (V)
BN-PAGE
1: wt
2: bcs1-F401I
3: bcs1-F401I + 5 µM ARTS

Figure 1

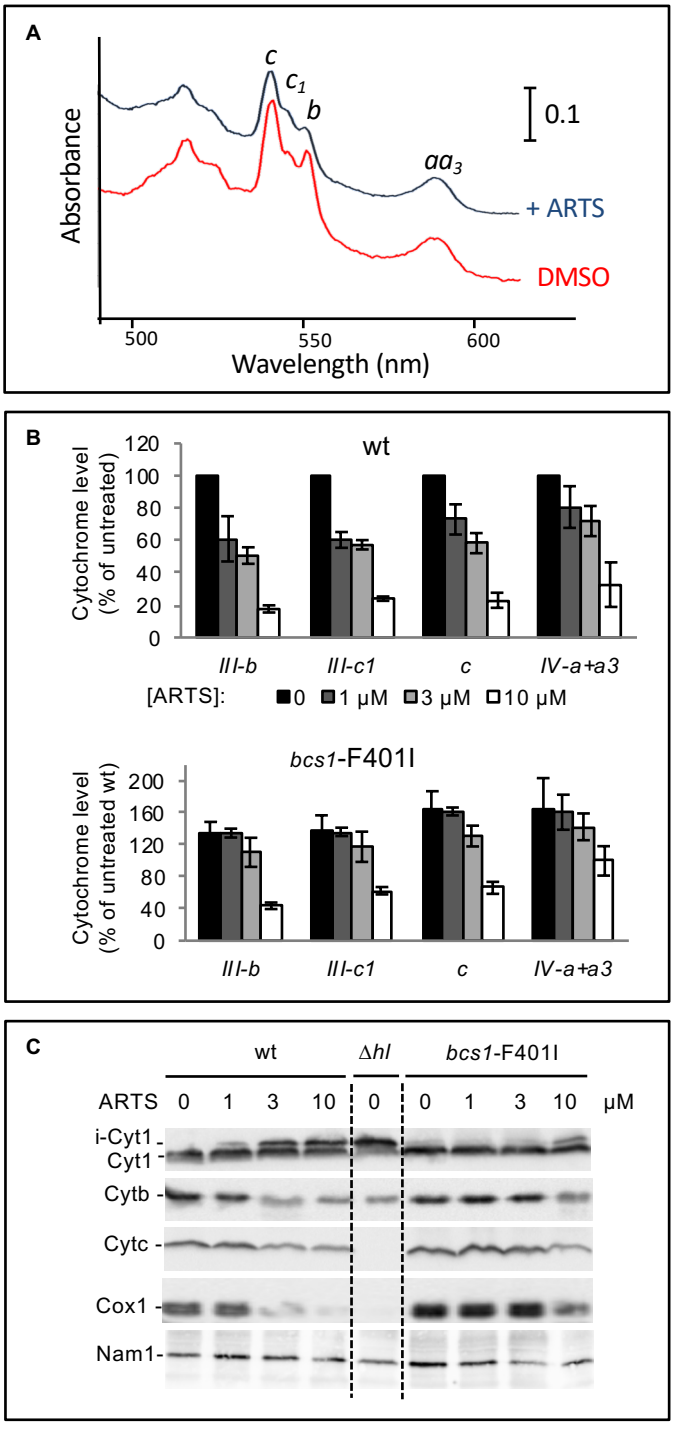
A
c
c1
b
aa3
0.1
+ ARTS
DMSO
Absorbance
500
550
600
Wavelength (nm)
B
wt
Cytochrome level (% of untreated)
120
100
80
60
40
20
0
III-b
III-c1
c
IV-a+a3
[ARTS]:
0
1 µM
3 µM
10 µM
bcs1-F401I
Cytochrome level (% of untreated wt)
200
160
120
80
40
0
III-b
III-c1
c
IV-a+a3
C
wt
Δhl
bcs1-F401I
ARTS
0
1
3
10
0
0
1
3
10
µM
i-Cyt1
Cyt1
Cytb
Cytc
Cox1
Nam1

Figure 2

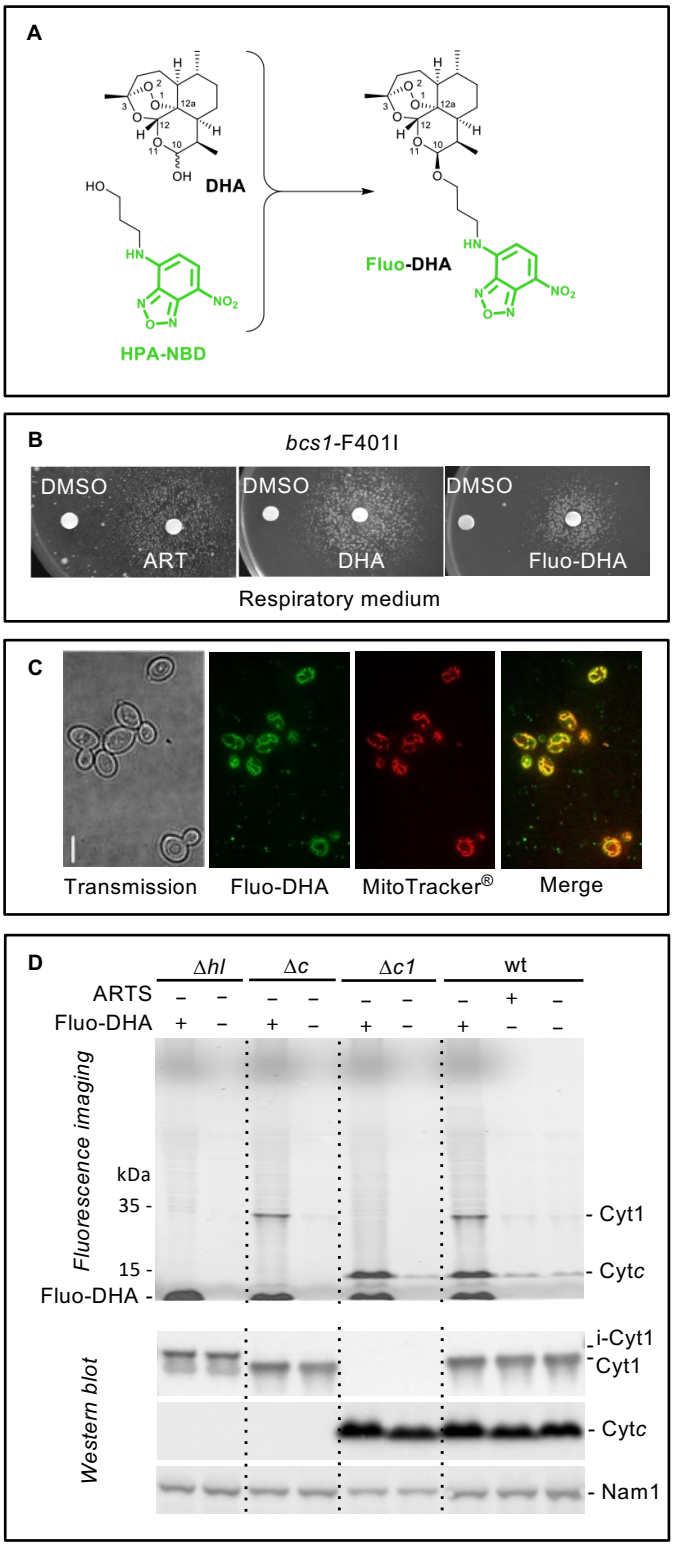
A
DHA
HPA-NBD
Fluo-DHA
B
bcs1-F401I
DMSO
ART
DMSO
DHA
DMSO
Fluo-DHA
Respiratory medium
C
Transmission
Fluo-DHA
MitoTracker®
Merge
D
Δhl
Δc
Δc1
wt
ARTS
Fluo-DHA
Fluorescence imaging
kDa
35 -
15 -
Fluo-DHA -
- Cyt1
- Cytc
Western blot
i-Cyt1
Cyt1
- Cytc
- Nam1

Figure 3

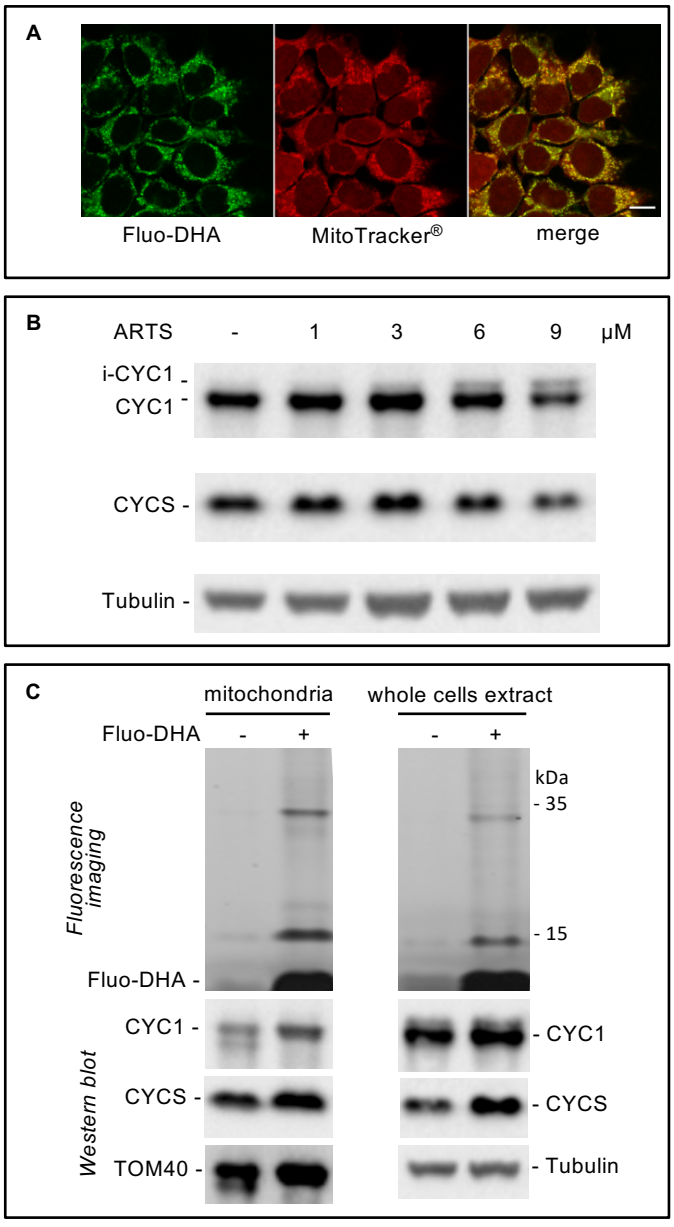
A
Fluo-DHA
MitoTracker®
merge
B
ARTS
-
1
3
6
9
µM
i-CYC1
CYC1
CYCS
Tubulin
C
mitochondria
whole cells extract
Fluo-DHA
-
+
-
+
kDa
35
15
Fluorescence imaging
Fluo-DHA
CYC1
CYCS
TOM40
Western blot
CYC1
CYCS
Tubulin

Figure 4

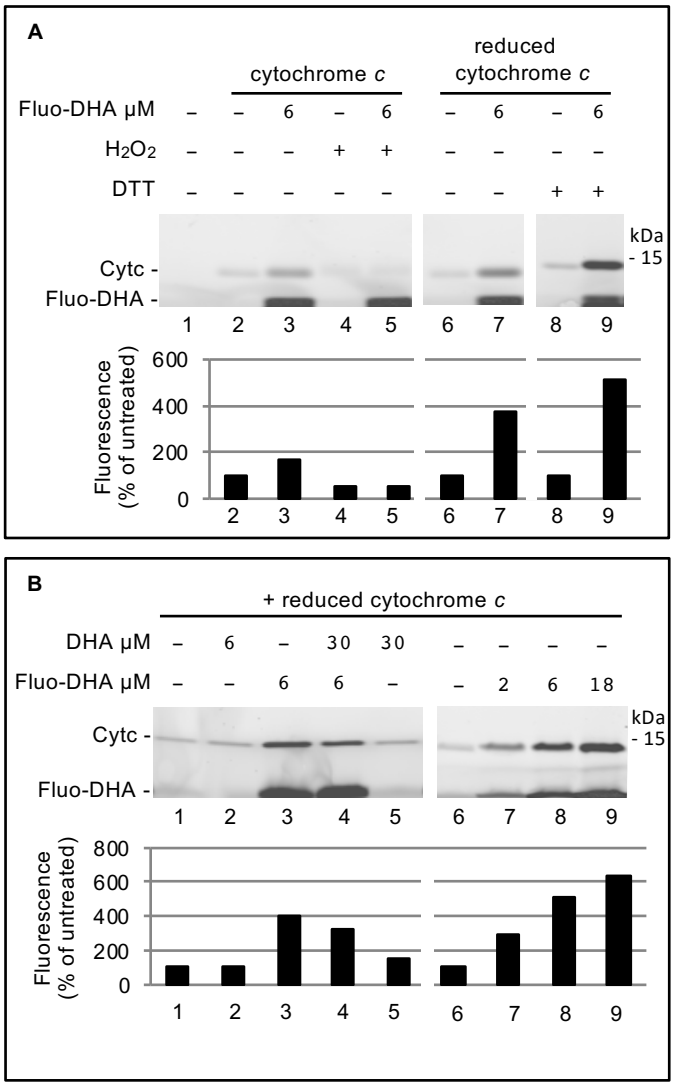
A
cytochrome c
reduced cytochrome c
Fluo-DHA µM – – 6 – 6 – 6 – 6
H2O2 – – – + + – – – –
DTT – – – – – – – + +
kDa
- 15
Cytc -
Fluo-DHA -
1 2 3 4 5 6 7 8 9
Fluorescence (% of untreated)
600
400
200
0
2 3 4 5 6 7 8 9
B
+ reduced cytochrome c
DHA µM – 6 – 30 30 – – – –
Fluo-DHA µM – – 6 6 – – 2 6 18
kDa
- 15
Cytc -
Fluo-DHA -
1 2 3 4 5 6 7 8 9
Fluorescence (% of untreated)
800
600
400
200
0
1 2 3 4 5 6 7 8 9

Figure 5

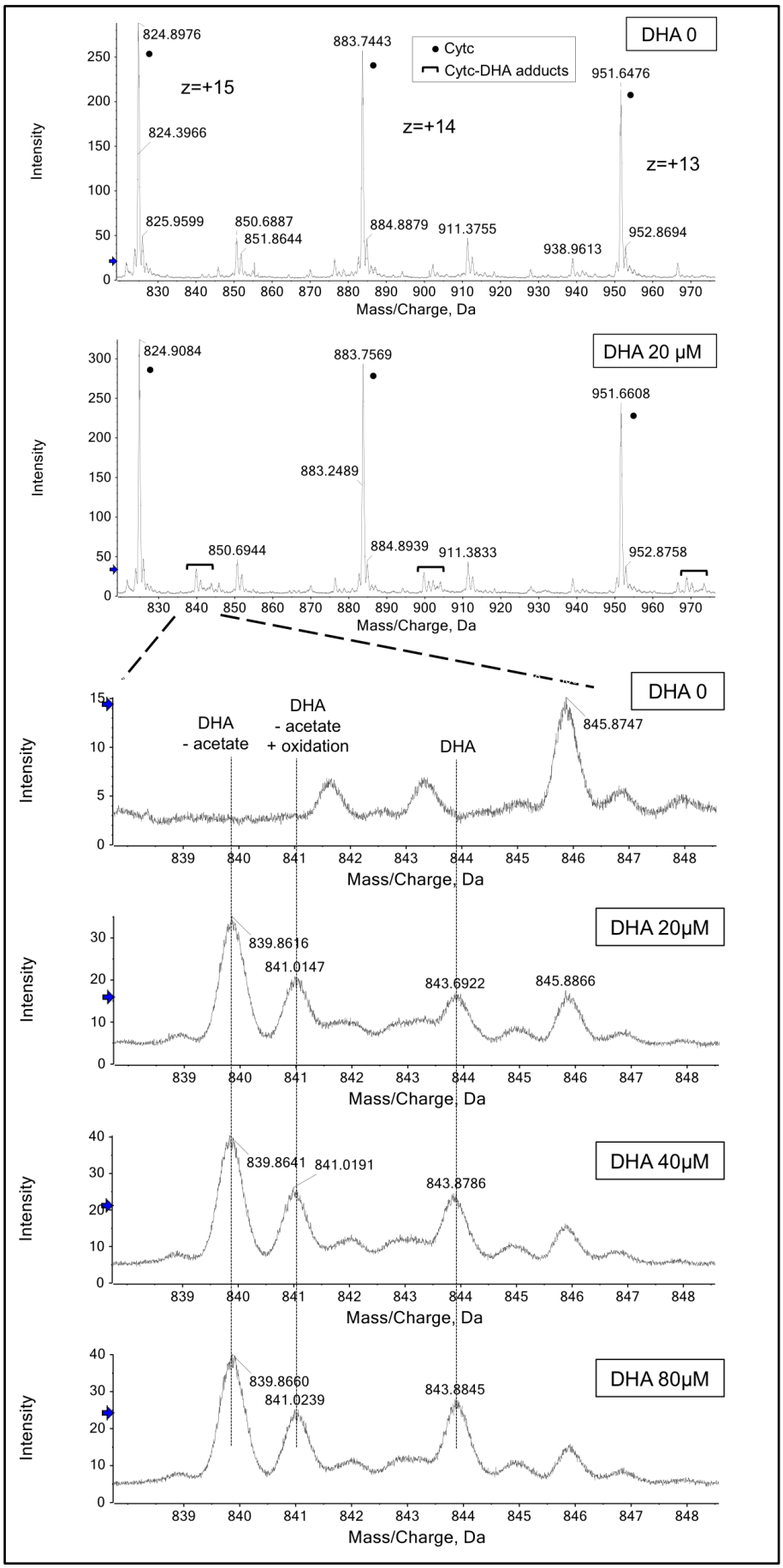
DHA 0
824.8976
883.7443
951.6476
Cytc
Cytc-DHA adducts
z=+15
z=+14
z=+13
824.3966
825.9599
850.6887
851.8644
884.8879
911.3755
938.9613
952.8694
Intensity
Mass/Charge, Da
DHA 20 µM
824.9084
883.7569
951.6608
883.2489
850.6944
884.8939
911.3833
952.8758
DHA 0
DHA
- acetate
DHA
- acetate
+ oxidation
DHA
845.8747
DHA 20µM
839.8616
841.0147
843.6922
845.8866
DHA 40µM
839.8641
841.0191
843.8786
DHA 80µM
839.8660
841.0239
843.8845

Figure 6

Supplementary material

Figure S1: Coimmunoprecipitation experiments of complex III subunits.

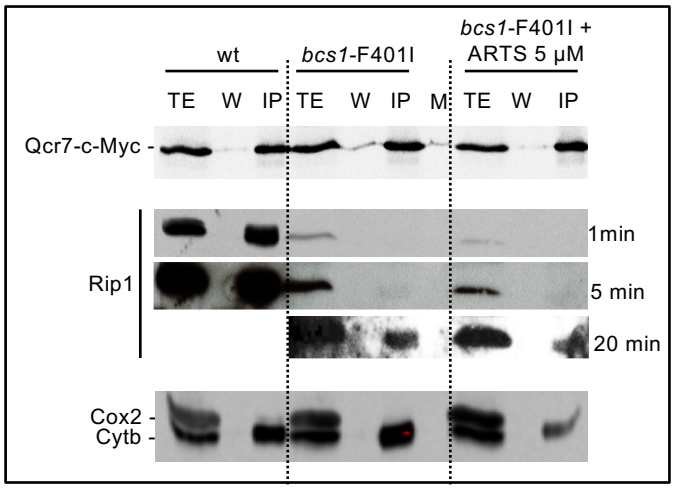

Legend of Figure S1:
Mitochondrial proteins were purified from wild-type or *bcs1*-F401I strains harboring a c-Myc tagged complex III subunit Qcr7, grown with or without 5 µM ARTS as indicated. The c-Myc tag was immuno-precipitated according to (Ostojić *et al.*, 2013), except that laurylmaltoside was used for the solubilization to get isolated respiratory complexes. The fractions were analyzed by SDS-PAGE and immunoblotted with antibodies against c-Myc and Rip1 as well as Cox2 and Cytb as controls. For Rip1 several exposures are presented. TE: total extract; W: washes; IP: immunoprecipitate. M: protein molecular mass markers.

Comments:
Efficient co-immunoprecipitation of Rip1 with Qcr7-c-Myc in the wild-type indicated the presence of a fully assembled complex III. In the *bcs1*-F401I mutant, very little Rip1 was detected, suggesting that most of the complex III forms that are co-immuno-precipitated with Qcr7-c-Myc are not fully mature. No difference in Rip1 level was observed with or without ARTS treatment. There is a little less cytochrome *b* after ARTS treatment, which is consistent with the decrease of pre-complex III observed after western blotting of BN-PAGE since pre-III always contains Cytb (Fig. 1D), and with the decrease of spectral cytochrome *b* (Fig.2B).

Figure S2: Maturation steps of the premature form of Cyt1 (pre-Cyt1).

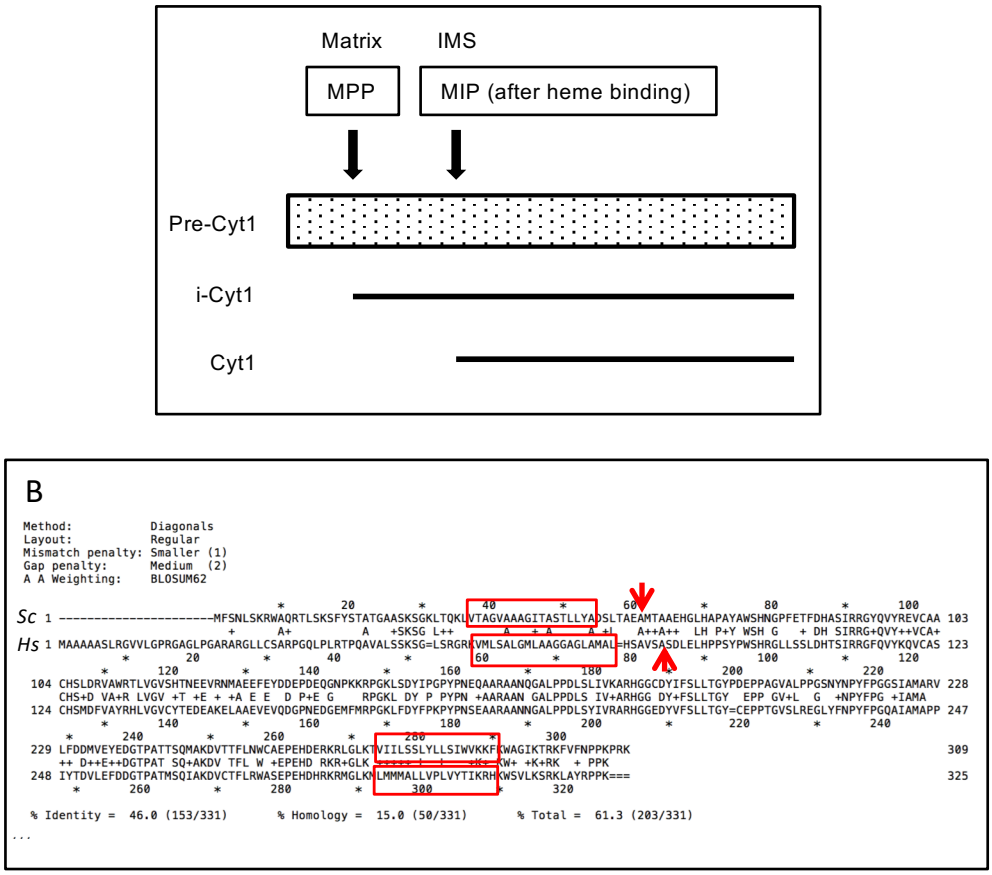

Legend of Figure S2:

Panel A: The first proteolytic cleavage by the matrix processing peptidase (MPP) occurs in the matrix to yield an intermediate form called i-Cyt1. The second cleavage by the mitochondrial intermediate protease (MIP) happens in the intermembrane space after attachment of the heme prosthetic group and generates the mature cytochrome *c1* (Cyt1) (Nicholson *et al.*, 1989; Arnold *et al.*, 1998).

Panel B: Sequence comparison of *S. cerevisiae* pre-Cyt1p *(Sc)* and human pre-Cyc1 (*Hs*) showing the conservation of hydrophobic stretches and of the position of the proteolytic processing site generating the mature cytochrome *c1*.

Figure S3: Alkylation and fragmentation pathway of DHA-cytochrome *c* adducts according to ESI-MS data.

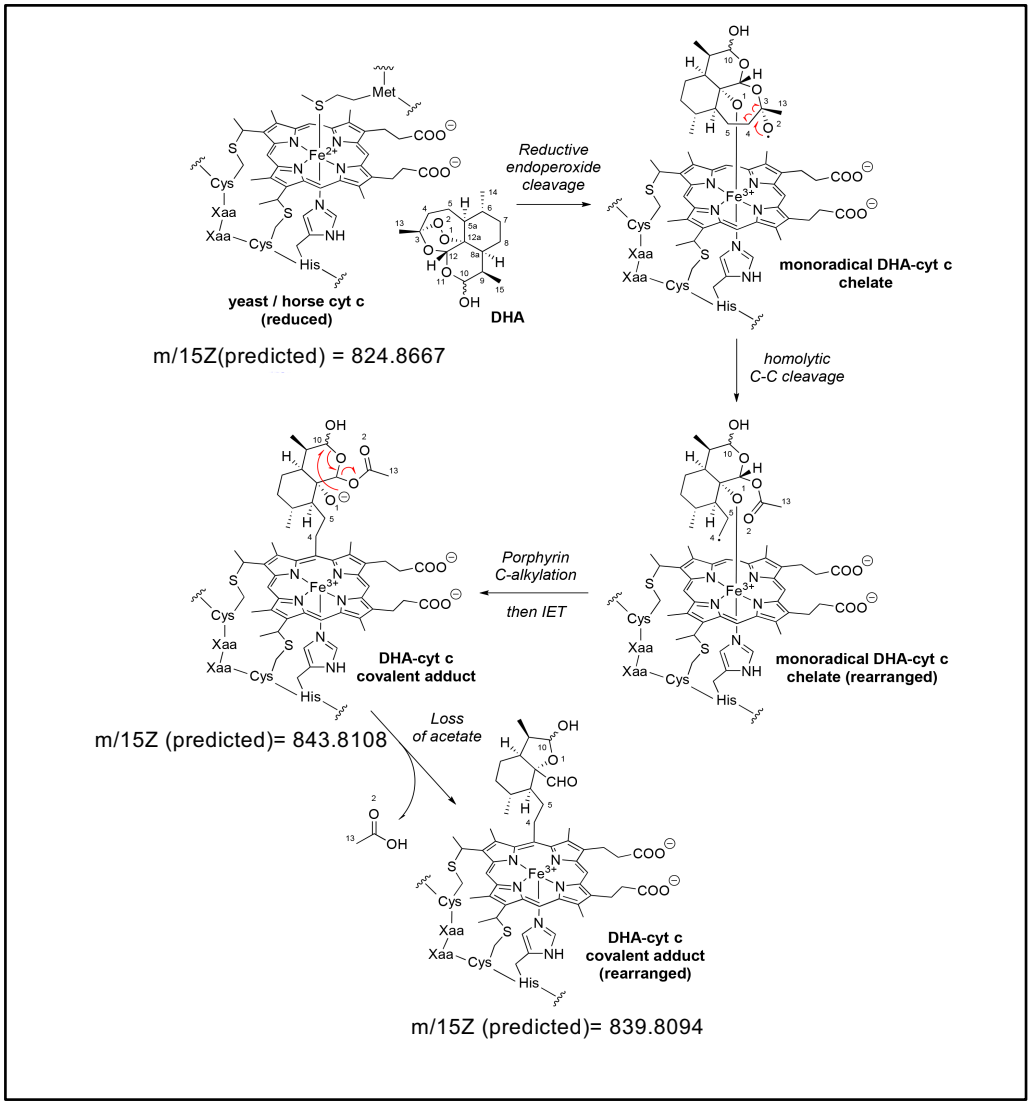

Legend of Figure S3:
Structure of horse cytochrome *c* was adapted from (Kleingardner & Bren, 2011) . Following displacement ligation by DHA, the coordinating Met residue was not further depicted in the figure. IET: intramolecular electron transfer.

		Peak intensity (z=+15)		
	m/z	+ 2.5 DHA	+ 5 DHA	+ 10 DHA
Cyt*c*	824.91	320	330	330
Cyt*c* + oxidation	825.97	47	48	47
Cyt*c* + DHA - acetate	839.86	35	40	40
Cyt*c* + DHA - acetate + oxidation	841.02	20	25	25
Cyt*c* + DHA	843.88	16	24	28
Total relative abundance of protein-DHA adduct (%)		**16.21**	**19.06**	**19.79**

		Peak intensity (z=+14)		
	m/z	+ 2.5 DHA	+ 5 DHA	+ 10 DHA
Cyt*c*	883.75	290	310	310
Cyt*c* + oxidation	884.89	45	45	42
Cyt*c* + DHA - acetate	899.78	31	36	35
Cyt*c* + DHA - acetate + oxidation	901.03	20	25	25
Cyt*c* + DHA	904	19	26	30
Total relative abundance of protein-DHA adduct (%)		**17.28**	**19.68**	**20.36**

		Peak intensity (z=+13)		
	m/z	+ 2.5 DHA	+ 5 DHA	+ 10 DHA
Cyt*c*	951.66	240	260	260
Cyt*c* + oxidation	952.88	39	39	36
Cyt*c* + DHA - acetate	968.92	25	29	29
Cyt*c* + DHA - acetate + oxidation	970.26	18	21	21
Cyt*c* + DHA	973.55	17	22	24
Total relative abundance of protein-DHA adduct (%)		**17.70**	**19.41**	**20.00**

Table S1. Mass spectrometry-based relative quantification of Cytochrome *c* (Cyt*c*) modification by DHA treated with different Cyt*c*:DHA ratios.

Relative abundance of Cyt*c*-DHA adducts to Cyt*c* was estimated for three charge states (z=+13, +14 and +15) by the ratios of the respective mass peak intensities. All different non-modified forms and DHA-protein adducts were considered to calculate total relative abundance. Oxide forms correspond to methionine oxidation. Means of total relative abundance for different DHA quantities were evaluated to represent 17.06 ± 0.77%, 19.38 ± 0.31% and 20.05 ± 0.29%, respectively for 1:2.5, 1:5 and 1:10 Cyt*c*:DHA ratios. The relative increase observed in total relative abundance as treated with more DHA quantities is mainly explained by the increase of DHA-Cyt*c* peak intensity.